Highly Efficient Biosensors by Using Well-Ordered ZnO/ZnS Core/Shell Nanotube Arrays

Highly Efficient Biosensors by Using Well-Ordered ZnO/ZnS Core/Shell Nanotube Arrays

Samar Tarish[1, 3], Yang Xu[1], Zhijie Wang[2], Faten Mate[3], Ahmed Al-Haddad[1, 3], Wenxin Wang[1] and Yong Lei[1,*]

[1] Institute for Physics and IMN MacroNano®, Ilmenau University of Technology, Professor-Schmidt-Straβe 26, 98693 Ilmenau, Germany.

[2] Key Laboratory of Semiconductor Materials Science, Institute of Semiconductors, CAS, Beijing 100083, P. R. China.

[3] Department of Physics, College of Science, University of Al-Mustansiriyah, Baghdad, Iraq.

[*] Email: yong.lei@tu-ilmenau.de

Abstract

We have studied the fabrication of the highly efficient glucose sensors by using well-ordered heterogeneous ZnO/ZnS core/shell nanotube arrays CSNAs. The modified electrodes exhibit a superior capability in electrochemical response towards ferrocyanide/ferricyanide and in glucose sensing. Further, the fabricated glucose biosensor exhibited good performance over an acceptable linear range from 2.39×10^{-5} to 2.66×10^{-4} mM, with a sensitivity as 188.34 mA mM^{-1} cm^{-2}, which is higher than those of the ZnO NAs counterpart. The low limit detection was realized to 24 μM is good over the electrodes based on the conventional structures. In addition, the enhanced direct electrochemistry of GOx indicates a fast electron transfer of ZnO/ZnS CSNAs electrode,

with a heterogeneous electron transfer rate constant (K_s) of 1.69 s^{-1}. The fast electron transfer attributed to the high conductivity of the modified electrodes. The presented ZnS shell can facilitate the construction of future sensors and enhance the ZnO surface in a biological environment.

Keywords: Glucose detection, Fast immobilization, High sensitivity, ZnO/ZnS structure, an electrochemical biosensor.

1. Introduction

Diabetes is an old disease that needs continuing medical care and patient self-management education to prevent acute complications and to minimize the hazard of long-term complications. In recent years, the number of diabetes patients rapidly increases all over the world and in turn monitoring glucose concentration has emerged as a critical health care issue. Thus, nowadays many researchers have focused on developing the strategies for accurate determination of glucose concentration. It is highly required to develop a cheap, simple, robust and rapid glucose biosensor with high sensitivity and lower limit of detection (LOD) [1,2]. Among the techniques for detecting glucose efficiently, the electrochemical method turns out to be standard. Various materials including metal oxides/sulfides and carbon have been proposed as efficacious blocks for constructing the according to electrodes. Ascribing to the low cost, high chemical stability, and nontoxic biocompatibility, ZnO and ZnS have received a substantial research attention. In addition, the high isoelectric points enable these materials to be ideal to immobilize enzyme with a low isoelectric point during the electrostatic

interaction. In order to load more bioactive materials and enhance the detecting resolutions, the heteronanostructure electrode is more advantageous than the planar counterpart. In particular, the electrode with heterogeneous nanostructure has gained extensive interests. The benefit arises from the dramatically increased surface area and the favorable kinetics of charge transfer. To avoid the performance instability from irregularly distributed of the conventional electrode for glucose sensing, the well-ordered nanostructure arrays fabricating is a great superiority for this purpose. Due to the well-controlled dimensional features, provide a good platform to optimize the sensing performance, among the various methods to prepare well-ordered nanostructure arrays based on anodic aluminum oxide (AAO). Powerful and diversity nanostructure arrays could be feasibly realized such as nanotubes, nanorods, and nanodot [3-10]. Not only in biosensors, these nanostructures could be widely used in protein separation and DNA sequencing [11,12], cell growth [13], tissue engineering and drug delivery [14]. Herein, we fabricated highly ordered ZnO/ZnS core/shell nanotube arrays (CSNAs) by using AAO template with atomic layer deposition (ALD) and rapid thermal deposition method. The resultant electrodes showed a higher electrochemical response to $[Fe(CN)_6]^{3-/4-}$ (FCN) than the ZnO nanotube arrays (NAs). For glucose sensing, the enzyme-modified electrode presented a lower LOD than the ZnO NAs counterpart and the previously reported electrodes.

2. Materials and methods

2.1 Materials

Glucose oxidase (E.C. 1.1.3.4) was purchased from Aspergillus Niger. Potassium hexacyanoferrate (III), $K_3Fe(CN)_6$ (99.98%), potassium hexacyanoferrate (II) trihydrate, $K_4Fe(CN)_6 \cdot 3H_2O$ (98.5%), Nafion (5 wt%), glutaraldehyde (50 wt %) and d(+)-glucose were purchased from Sigma-Aldrich. Potassium chloride (KCl 99.0%) was purchased from VWR (NASDAQ: VWR) and Phosphate buffered (PBS) 0.1 M solution was prepared from Na_2HPO_4 and KH_2PO_4 (VWR) solution with NaCl, the pH was adjusted to 7.4. The materials were used without any further purification.

2.2 Methods

The anodic aluminium oxide (AAO) templates were fabricated by means of a two-step anodization method as shown in (Figure 1: step 1) by using high-purity (99.99%) aluminium foil as the starting material. The ZnO nanotube arrays on (AAO) templates (Figure 1: step 2) were grown by a PicoSun ALD system. This procedure was repeated for 250 to 300 cycles according to the desired wall thickness of ZnO nanotubes as described in details in our previous reports [15,16]. Then, the ZnO/AAO nanotube samples were immersed in 0.01 M sodium sulfide (Na_2S) (98%, Aldrich) solution at 60^{o}C for 60 min to get ZnS shell thickness about 12 nm, this procedure could remove the AAO simultaneously as shown in (Figure 1 step: 3) [15]. The top surfaces of ZnO/AAO NAs and ZnO/ZnS CSNAs were initially evaporated with a thin layer of Zn (10 nm), then a 30 nm Au layer was deposited on ZnO/AAO/Zn or ZnO/ZnS/Zn by electron beam deposition (Kurt J. Lesker PVD225, deposition rate 0.2 Å/s). Thereafter a thick layer of Ni was evaporated to support the surface of the sample during the removal of Al foil. The Al backside was removed by a mixture solution of $CuCl_2$ (85 wt %) and HCl (15 wt %).

Then, the AAO template was removed from ZnO/AAO/Zn/Au/Ni by using NaOH solution (0.1 M) at 40^{o}C (Figure1: step 4). The samples were initially connected to the copper wire by using a silver paste conducting. Afterward, the silver paste layer was fully coated with varnish protective coating.

Initially, the sensor electrodes as illustrates in Figure 1 are investigated with respect to the electrochemical response towards ferrocyanide/ferricyanide $[Fe(CN)_6]^{3-/4-}$ 1.0 mM standard redox system in aqueous 0.1 M KCl solution, to investigate the surface modification. For the immobilization process, 10 µL of GOx solution 20 mg mL^{-1} was prepared in 0.01 M PBS (pH 7.4), afterward was drop-coated on the top of the two electrodes. The whole electrode was dried at room temperature for 24 h (Figure 1: step 5). Before the immobilization of the enzyme, the electrodes were rinsed with PBS to generate a hydrophilic surface [11]. The cross-linking procedure was performed by adding 10 µL aqueous solutions containing 2.5% glutaraldehyde and 0.5% Nafion onto the electrodes surface, and the electrode was dried at 23±2°C (Figure 1: step 6). The sensor electrodes were stored at 4 ^{o}C before usage. After completing these steps, a cyclic voltammetry method was applied by using a computer-controlled system (EC-Lab software V10-19) at room temperature. A conventional three-electrode system of working electrode (WE), reference (Ag/AgCl) electrode (RE) and counter electrode (CE) were used as the electrochemical cell setup as presented in Figure S1a. To study the behavior at the electrode/electrolyte interface we require both potential and current to be monitored as illustrated in the simplified diagram in Figure S1b. In this cell the current moves between the WE and the CE. In the same time the potential difference between RE and WE is controlled all the time during the measurement. The potential between the WE and CE

usually is not measured. This is the voltage applied by the control amplifier and it is limited by the compliance voltage of the instrument, so that the potential difference between the WE and RE will be equal to the potential difference. This configuration allows the potential across the electrochemical interface at the WE to be controlled with respect to the RE. The cyclic voltammograms (CV) curves were recorded in the potential range from −0.1V to +0.5 V and −1V to +1V vs. Ag/AgCl for $[Fe(CN)_6]^{3-/4-}$ and glucose, respectively. The scan rates (ν) during the experiments ranging is from 0.02 - 0.12 V s^{-1}.

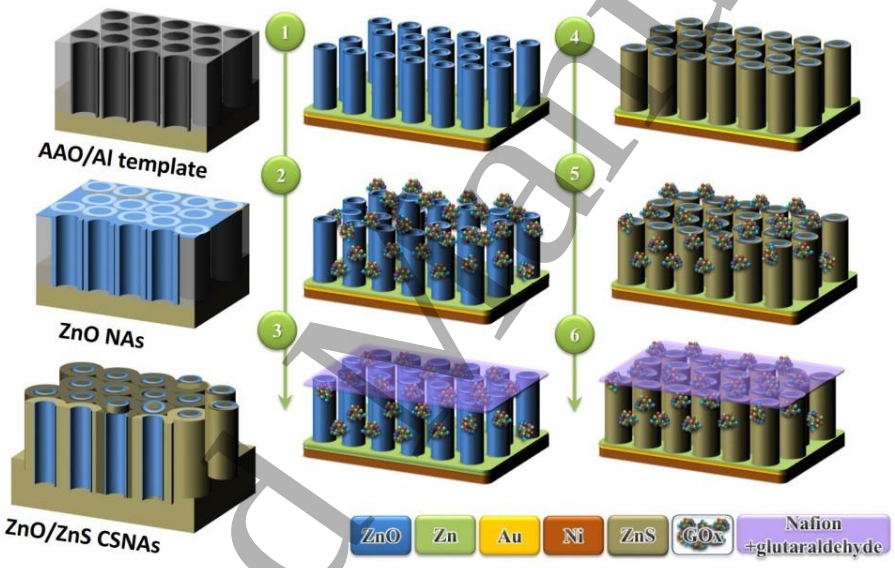

Figure 1. Schematic diagram of the biosensor. In steps (1-3) is the synthesis of highly ordered nanotube arrays AAO templates, ZnO NAs and ZnO/ZnS CSNAs. In steps (4-6) is the preparation of the electrodes for the electrochemical process on the surface and inner wall of the nanotubes. In step (4) is the removal of AAO templates after depositing Zn, Au, and Ni layers. In step (5) is the immobilization of enzyme glucose oxidase (GOx) on the surface of the sensor electrodes. In step (6) is the coating of glutaraldehyde and Nafion solution onto the electrodes surface. The active site of the glucose oxidase catalyzed a reaction on the electrodes as illustrates in step (6).

3. Results and Discussion

3.1 Characterization of ZnO NAs and ZnO/ZnS CSNAs electrodes

Figure 2a shows a representative of the typical scanning electron microscopy (SEM) images of the nanopore arrays, in which an array of well-ordered alumina pores could be clearly observed with a high regularity, large scale and without defects. The average diameter of the pores is around 70 nm, with a thickness of 1800 nm. Figure 2b exhibits the ZnO nanotube array prepared by a typical ALD procedure. The ZnO freestanding nanotube after the AAO was removed as shown in Figure 2c the wall thickness of the ZnO is estimated around 18 nm associated with ALD cycles. Figure 2d presents the ZnO/ZnS, the shell thickness around 12 nm belongs to sulfidation time. These electrodes with well-ordered nanostructure offer a good scaffold to load bioactive materials and increase the according to sensitivity. Figure 2e shows the cross sectional of the ZnO/ZnS CSNAs after loading of 10 μL glucose oxidase solution with a high uniform coverage of Nafion-glutaraldehyde solution in the wall nanotubes could be concluded. The presence of the biomaterials of the enzyme and the Nafion could also be supported by EDX patterns as shown in Figure 2f.

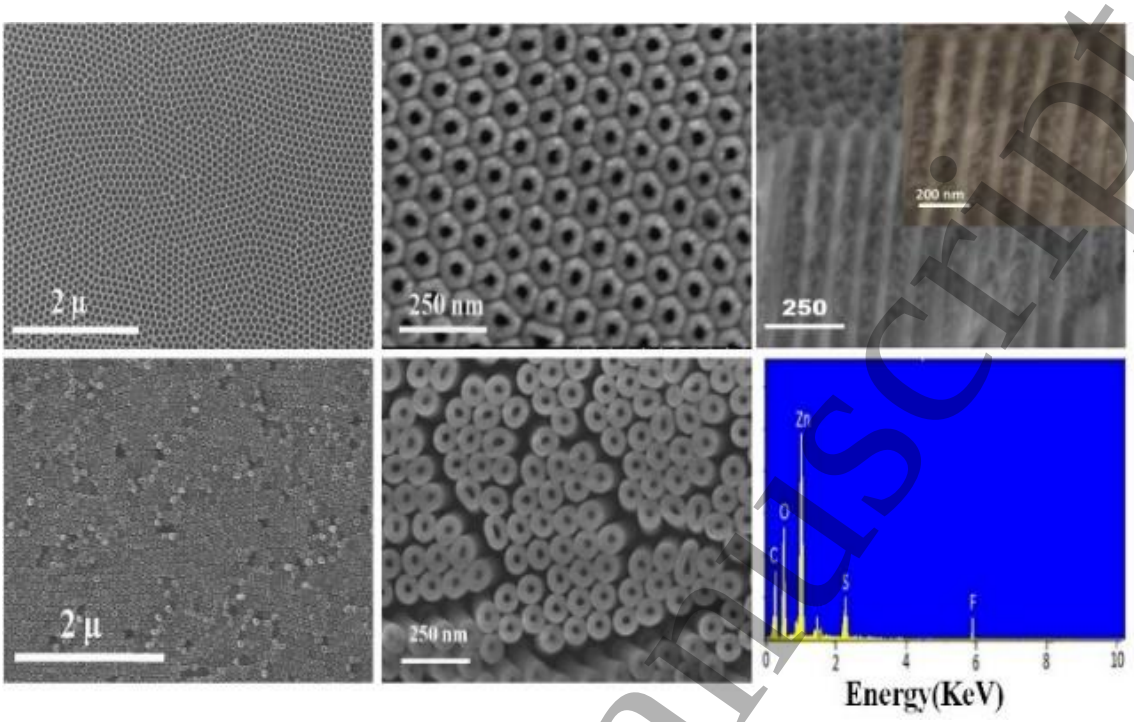

Figure 2. (a) SEM image of the AAO template with a high regularity before deposing ZnO. (b) ZnO NAs after 300 cycles of ALD deposition at 250°C with the inset of cross-section view. (c) SEM image of bare ZnO nanotube arrays after removing AAO template with NaOH (0.1 M) solution. (d) ZnO/ZnS CSNAs array after 50 min sulfidation time. (e) ZnO/ZnS CSNAs after depositing of Nafion with glutaraldehyde. (f) EDX spectrum.

3.2 Electrochemical performance of ZnO NAs and ZnO/ZnS CSNAs toward $[Fe(CN)_6]^{3-/4-}$

Prior, to all experiments the solutions were purged with high–purity nitrogen to eliminate the dissolved oxygen. The CVs curves presented in Figure 3a and b show some interesting characteristics. Firstly, it is obvious that the electrochemical peaks oxidation of the $[Fe(CN)_6]^{3-/4-}$ solution on ZnO and ZnO/ZnS surface are clearly separated from each other.

Upon increasing the concentration of $[Fe(CN)_6]^{3-/4-}$, its oxidation peak currents enhance, indicating the effect of the change of concentration at 7.93×10^{-5}-2.15×10^{-4} mM at the scan rate of 0.05 V s^{-1}. The ratio of the observed currents at reverse and forward scans is equal to the relation ($\frac{i_p^{ox}}{i_p^{red}}$ =1.0), pointing that there are no chemical reactions coupled to the electrode process, and confirm the charge-transfer process is completely reversible (it is well known that such reactions can largely raise the ratio of peak currents). The oxidation potential of bare ZnO is 0.078 V vs. Ag/AgCl, while for ZnO/ZnS is about 0.061 V. This could be attributing to the difference in the surface chemistry of the two materials, and could improve the electrochemical response of heterogeneous nanostructures. The CVs curves of the ZnO electrode look somehow noisy and the current at the oxidation peak current is around 0.0158 mA whereas, the curves of the ZnO/ZnS electrode are smooth and the oxidation peak current is up to 0.226 mA. This indicates that the ZnO/ZnS is superior over ZnO in electrochemical response. The plots of anodic current versus $[Fe(CN)_6]^{3-/4-}$ concentration are given in Figure 3c and 3d, and the current increases with increasing the concentration. The error bars in Figure S2 display the standard deviations of the measured data for the ZnO NAs and ZnO/ZnS CSNAs and it represents the 95% confidence intervals of the average value. It is our delight to write the ZnO/ZnS CSNAs showed 2 times higher sensitivity (333.4 mA mM^{-1} cm^{-2}) in comparison with ZnO NAs (151.81 mA mM^{-1} cm^{-2}), by calculating the slope from the linear portion of the plots in Figure 3c and d. The limit of detection (LOD) was calculated from the formula ($3\times\sigma \mid$ slope), σ is the standard deviation of the current density [17,18].

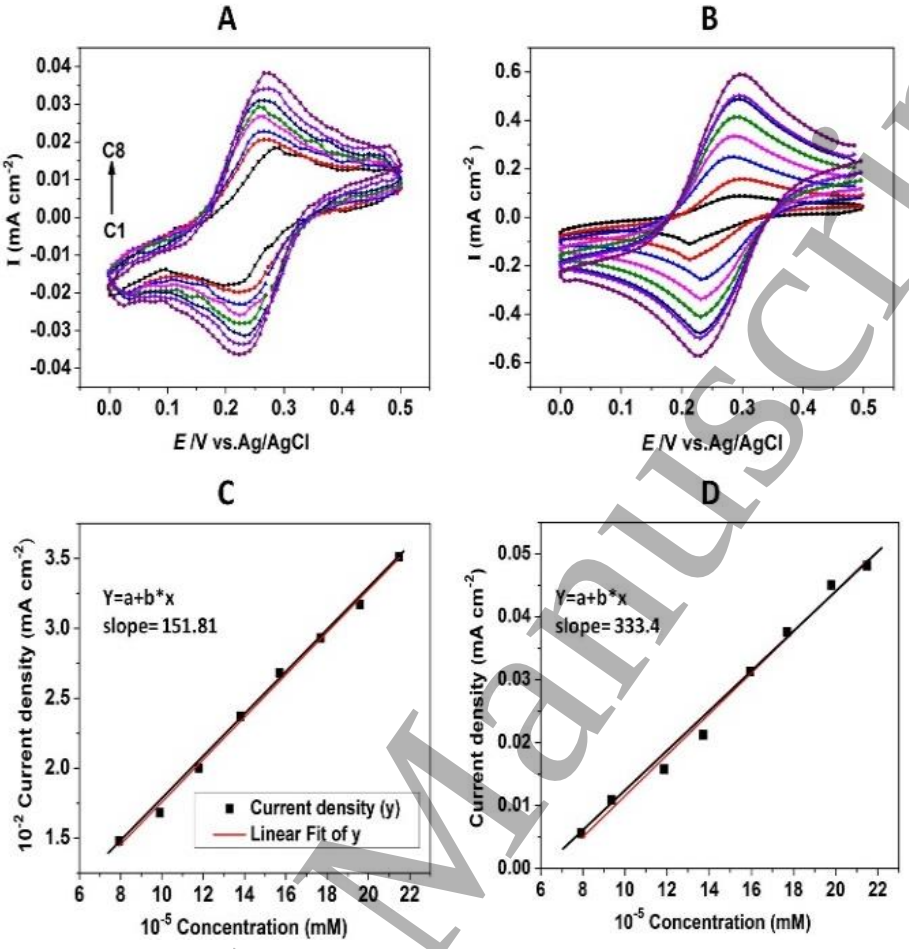

Figure 3. CVs spectra measured in range concentration (from C1=7.93×10^{-5} to C8=2.15×10^{-4}) mM of $[Fe(CN)_6]^{3-/4-}$ in (0.1 M KCl) at the scan rate=0.05 V s^{-1} on (a) ZnO NAs and (b) ZnO/ZnS CSNAs. The corresponding sensitivity and the lower limit of detection are present in (c) and (d), respectively.

It was found that the LOD of CSNAs as 24 μM is lower than NAs 31 μM at a lower concentration of 7.93×10^{-5} mol L^{-1}, which means that the modified sensors are sensitive to lower concentrations and higher modification. The sensors are sensitive to lower concentrations. The variation of electrochemical responses with scan rate is studied in briefly. Figure 4a and b represent the CVs recorded at different scan rates (0.02-0.12 V s^{-1}) under constant concentration 1.38×10^{-4} mol L^{-1} of $[Fe(CN)_6]^{3-/4-}$. A linear

relationship was realized between the reduction peak and oxidation peak currents (i_{pred} and i_{pox}) with the square root of scan rate as presents in Figure 4c and d. Upon increasing the scan rates, the redox peak currents and peak separation increase linearly. Meanwhile, the cathodic peak and anodic peak currents show a small shift with the following increase in the peak-to-peak separation. Particularly, the anodic and cathodic peak of potential separation ΔE_p of the bare ZnO NAs was found to vary with the concentration of the electroactive compound $[Fe(CN)_6]^{3-/4-}$ as shown in Figure 5a and b (red curve). Namely, the increase of the potential separation ΔE_p with the concentration increasing to finally reach the value of ΔE_p is 0.102 V at scan rate v= 0.05 V s^{-1} for the concentration 2.15×10^{-4} mol L^{-1}.

Whereas the peak potential separation ΔE_p of ZnO/ZnS CSNAs was recorded as 0.114 V at the same concentration and scan rate. It is obvious that the ΔE_p values obtained on ZnO/ZnS CSNAs (0.089 V) are smaller than those determined on ZnO NAs thus, showing somewhat higher electron transfer kinetics in ZnO/ZnS CSNAs. However, the electron transfer kinetics are independent with the concentration of the electroactive compound while the effect of the uncompensated resistance dependents on concentration. The results indicated that the increase of ΔE_p with concentration could be mainly attributed to resistance effects namely, to the resistance that remains uncompensated [19]. By using the Nicholson relation [20]. The heterogeneous electron transfer constant (K_s) of $[Fe(CN)_6]^{3-/4-}$ was calculated in the investigated concentrations and scan rates.

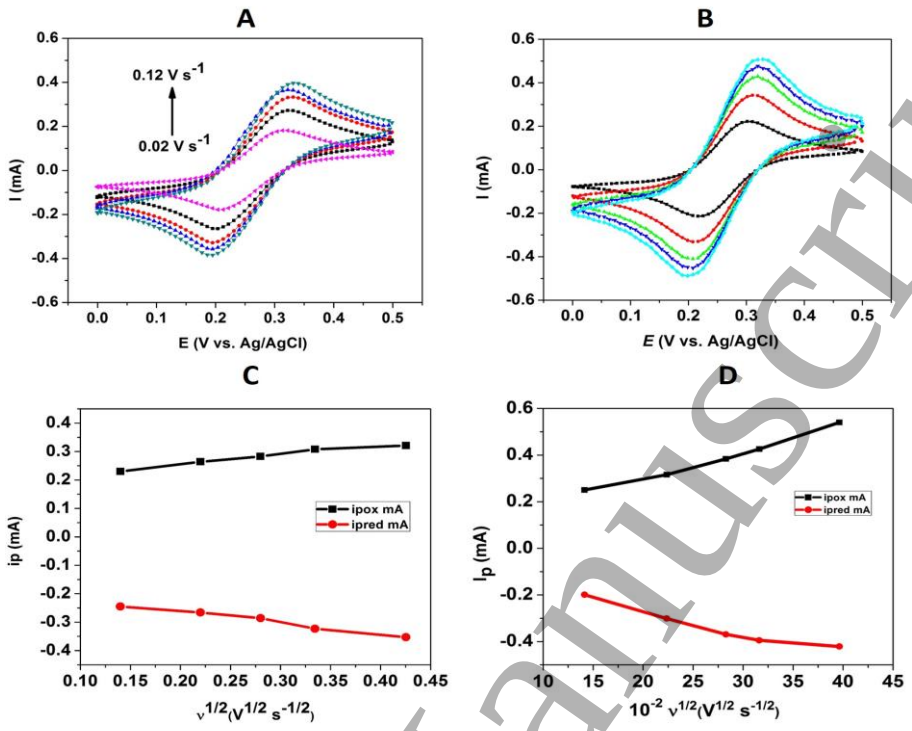

Figure 4. CVs spectra of ZnO–$[Fe(CN)_6]^{3-/4-}$ (a) and ZnO/ZnS $[Fe(CN)_6]^{3-/4-}$ (b) at different scan rate (0.02-0.12 V s^{-1}). (c and d) Curves present the linearity peak current with the square root of scan rate, labeled by the oxidation peak current i_{pox} and the reduction current i_{pred}.

The results reveal that the variation of Ks with the concentration is the inverse with ΔE_p as shown in Figure 5a and b (blue curve). Specifically, the value of $K_s=6.12\times10^{-3}$ cm s^{-1} for ZnO measured initially for $C=7.93\times10^{-5}$ mol L^{-1} at scan rate of 0.05 V s^{-1}.

Gradually, the decrease K_s with the increase of the electro-active compound concentration to reach the final value of $K_s=4.34\times10^{-3}$ cm s^{-1} at $C=2.15\times10^{-4}$ mol L^{-1}, under scan rate $\nu=0.05$ V s^{-1}. In contrast, it is very interesting that the value of K_s of the ZnO/ZnS CSNAs of $K_s = 23.4\times10^{-3}$ cm s^{-1} in the concentration range of 7.93×10^{-5}-2.15×10^{-4} mol L^{-1}, is higher than the K_s of ZnO under at the same measurements as shown in Figure 5a and b (curve blue). Furthermore, the real surface active area of the

electrode (A) was calculated from the slope of concentration–current calibration curve at the constant of scan rate (ν) as shown in Figure 4c and d, according to the Randles-Sevcik equation [21].

$$i_p = (2.69 \times 10^5) n^{3/2} A \, D^{1/2} C_i \nu^{1/2} \quad (1)$$

Here, *n* and *A* represent the number of electrons transferred (n=1) and *A* the active area of the electrode (cm^2), respectively, *F* is the Faraday's constant (96485 coulombs/mole). The concentration of the $[Fe(CN)_6]^{3-/4-}$ is denoted by C where the diffusion coefficient ($cm^2\ s^{-1}$) and time (s) are denoted by (D_{ox}=7.63×10^{-6} $cm^2\ s_{-1}$), *ν* is the scan rate ($V\ s^{-1}$). Thus, the active area of the ZnO NAs based electrode is calculated to be 0.44 cm^2 and that of ZnO/ZnS CSNAs electrode is 0.41 cm^2. The active area of ZnO/ZnS CSNAs is smaller than that of ZnO NAs due to the enlargement of nanostructure size during the ZnS shell formation.

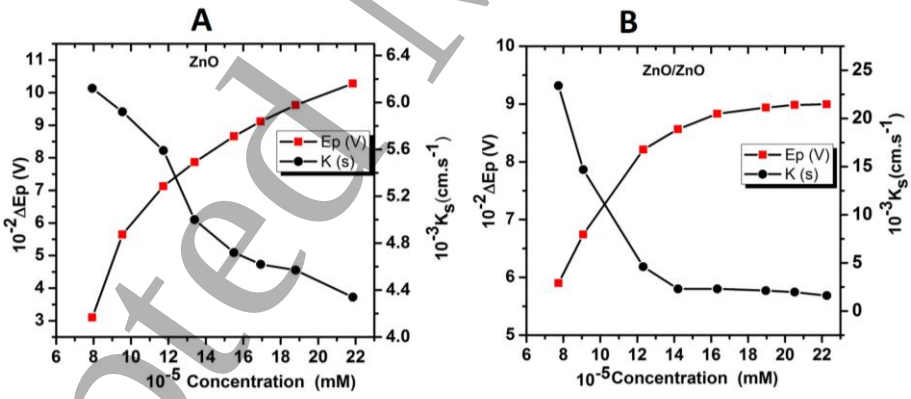

Figure 5. Variation of peak potential separation (red curve) and heterogeneous electron transfer rate constant (blue curve) with concentration in CVs recorded on either ZnO NAs (a) or ZnO/ZnS CSNAs (b) for $[Fe(CN)_6]^{3-/4-}$ solutions (0.1 M KCl) at ν = 0.05 $V\ s^{-1}$.

3.3 Electrochemistry measurement of glucose sensing

Owing to the advantages of the nanostructure arrays, the biosensor performance was analyzed by the cyclic voltammograms CVs of GOx in the concentration range of 2.45×10^{-5}-2.66×10^{-4} mM. Figure 6 displays the CVs curves acquired at the bare electrode (a) and the modified electrodes (b) at a scan rate of 50 mV s^{-1}.

The CVs curves are evidenced that the ZnO/ZnS CSNAs recorded high current response comparing with the ZnO NAs. The GOx immobilized electrodes exhibit a pair of standard redox peaks for glucose sensing and the peaks positions are in agreement with previous reports [22,23]. The formal potentials are 0.485 V and 0.344 V were realized from ZnO NAs and ZnO/ZnS CSNAs based electrodes, respectively. The CVs have displayed a quasi-reversible electrochemical redox peak; it is attributed to the electron transfer of redox active sites in GOx. The active site of this enzyme is a flavin adenine nucleotide (FAD) that exists in one of two forms-oxidized (FAD) or reduced ($FADH_2$). FAD oxidizes glucose to gluconic acid, and the $FADH_2$ generated by this reaction can be oxidized to FAD by oxygen (hydrogen peroxide is a by-product of this reaction). This mechanism is shown in Figure 1 (Step 4). The GOx catalyzed reaction can be described as following the reaction [24-26]:

$$GOx + FAD + 2e^- + 2H^+ \leftrightarrow GOx + FADH_2 \quad (2)$$

$$GOx-(FAD) + Glucose + O_2 \longrightarrow GOx-(FAD) + Gluconolactone + H_2O_2 \quad (3)$$

It is worth mentioning that the fabricated ZnO/ZnS CSNAs was recorded the higher sensitivity (188.34 mA mM^{-1} cm^{-2}) in comparison with ZnO NAs (153.73 mA mM^{-1} cm^{-2}). The limit detection (LOD) were realized to 0.42 µM and 0.29 µM for ZnO NAs and ZnO/ZnS CSNAs respectively, were calculated from the slopes between the anodic current density and the variation of concentration as shown in Figure 6 c and d. The

sensitivity improvement is attributed to the role of the ZnS shell and the heterojunction structure is beneficial for transporting the charges efficiently. The effect of scan rate on the GOx/ZnO nanotubes and GOx/ZnO/ZnS CSNAs electrodes with concentration 12.19 μM at scan rate from 0.2 to 0.12 V s^{-1} is illustrated Figure S3. The oxidation peak current i_{pox} and reduction peak current i_{pred} show a linear relationship with increasing the scan rates, showing that the redox reaction of GOx at the composite electrode is a typical surface-controlled quasi-reversible process. The sensitivity and limit detection of glucose detection for the ZnO/ZnS CSNAs is significantly high when comparing with other previously reported glucose biosensors based on differently modified working electrodes, as shown in Table S1. The reference performances are cited from the literatures previously reported. Thus, a superior performance of our biosensors over the reported ones could be concluded. The heterogeneous electron transfer constant (K_s) of GOx/ZnO nanoarrays NAs for GOx/ZnO/ZnS CSNAs electrodes has been calculated by using Laviron's equation [27].

$$Log\ Ks = \alpha Log(1-\alpha) Log\alpha - Log(RT/nF\nu) - \alpha(1-\alpha)nF\Delta E_p/2.3RT \quad (4)$$

Where: α is a dimensionless parameter known as electron transfer coefficient, n is the number of electrons involved in redox process (n = 2), F is Faraday constant (96485 C mol^{-1}), ν is scan rate (0.05 V s^{-1}), R is a gas constant (8.314 J mol^{-1} K^{-1}), T is a temperature in K (T=293 K). ΔEp is the peak separation of the $FAD/FADH_2$ redox couple. The value of α is 0.46 that could be calculated from the slopes of anodic (E_{pa}) and the cathodic (E_{pc}) peaks potentials vs. scan rate. The K_s value of the GOx immobilized ZnO/ZnS CSNAs is recorded as (1.65 s^{-1}) higher than that of the bare ZnO NAs (0.95 s^{-1}). The high conductivity and good microenvironment of the ZnO/ZnS CSNAs facilitate

the direct electron transfer between the enzyme matrix and the electrode surface. The value (ks) of ZnO/ZnS CSNAs is very close to the values that reported previously on Multiwall carbon nanotubes based ZnO (MWCNT) (1.66 s^{-1}) [28], and MWCNT within a dihexadecyl phosphate (1.69 s^{-1}) [29], higher than those reported on boron-doped MWCNTs (1.56 s^{-1}) [24], MWCNTs modified with gold (1.08 s^{-1}) [30], and CNTs modified (1.53 s^{-1}) [31].

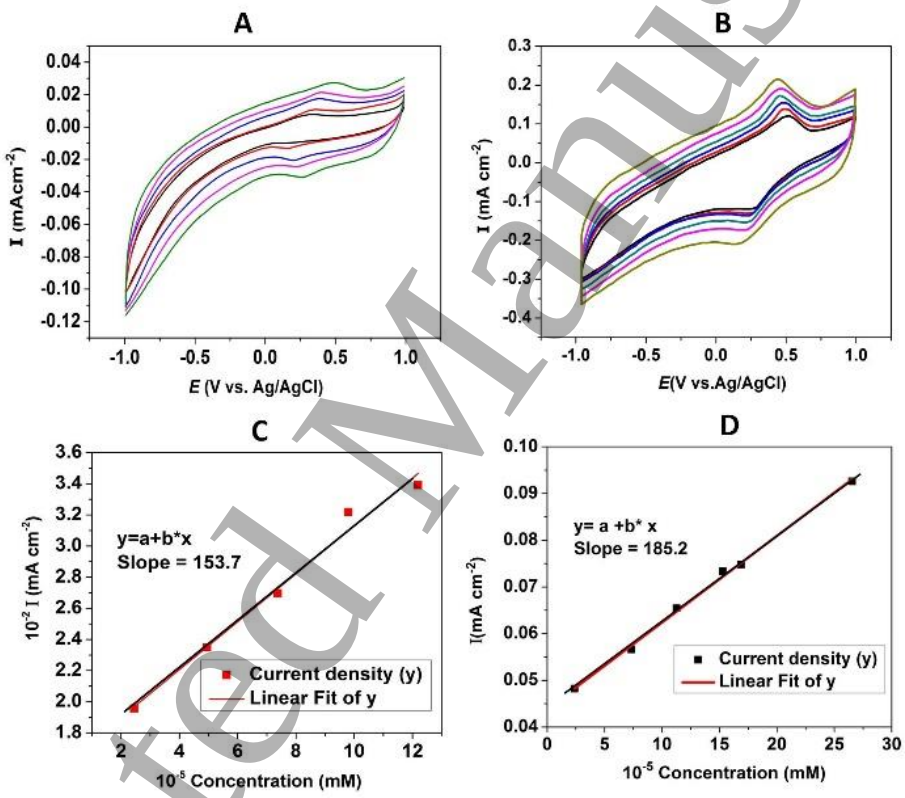

Figure 6. Cyclic voltammogram of bare ZnO NAs (a) and ZnO/ZnS CSNAs (b) in PBS (0.01M) at scan rate 50 V s^{-1} were measured in the potential range from −1 to +1 V. Variation of oxidation peak current density with concentration of glucose recorded in CVs on either ZnO NAs (c) or ZnO/ZnS CSNAs (d).

The electric circuit that demonstrates how the two electrodes ZnO NAs and ZnS/ZnO CSNAs nanotube arrays are used of the sensor is illustrated in the simplified diagram in

Figure S3. The circuit controls the potential of the working electrode and turns into the signal current to a voltage is named a potentiostat. By operational amplifier A2, the signal (current) from the working electrode is converted to a voltage. This circuit also controls the potential of the working electrode at the bias potential, V bias. The reference electrode potential is compared to the stable input potential, V bias. At the counter electrode, the operational amplifier A1 produces a potential which is just sufficient to produce a current that is quite equal and reverse of the working electrode current. On the other hand, a constant voltage is preserved between the working and the reference electrodes.

4. Conclusions

We have constructed glucose sensors based on well-ordered ZnO/ZnS CSNAs. The advanced heterogeneous nanostructure is better than the ZnO NAs counterparts are in term of electrochemical response towards FCN. As for the glucose sensing, a high sensing performance of the ZnO/ZnS CSNAs electrode over ZnO NAs based devices and other reported sensors is realized. We hope that our work could ascend future attentions on using well-ordered nanoarrays for glucose sensors and might be transferred to other applications in the field of sensors.

Acknowledgements

This work is financially supported by the European Research Council (ThreeDsurface: 240144), BMBF (ZIK-3DNanoDevice: 03Z1MN11), BMBF (Meta-ZIK-BioLithoMorphie: 03Z1M512) and Deutsche Forschungsgemeinschaft (DFG: LE 2249_4-1).

References

[1] Giri A K, Charan C, Saha A, Shahi V K and Panda A B 2014 An amperometric cholesterol biosensor with excellent sensitivity and limit of detection based on an enzyme-immobilized microtubular ZnO@ZnS heterostructure *J. Mater. Chem. A* **2 16997–17004**

[2] Xia L, Song J, Xu R, Liu D, Dong B, Xu L and Song H 2014 Zinc oxide inverse opal electrodes modified by glucose oxidase for electrochemical and photoelectrochemical biosensor *Biosens. Bioelectron.* **59 350–357**

[3] Shi L, Xu Y and Li Q 2010 Controlled fabrication of SnO_2 arrays of well-aligned nanotubes and nanowires *Nanoscale.* **2 2104–2108**

[4] Wang Z, Cao D, Xu R, Qu S, Wang Z and Lei Y 2016 Realizing ordered arrays of nanostructures: A versatile platform for converting and storing energy efficiently *Nano Energy*. **19 328–362**

[5] Liu D, Wang L, Ma S, Jiang Z, Yang B, Han X and Liu S 2015 A Novel Electrochemiluminescent Immunosensor Based on CdS-Coated ZnO Nanorod Arrays for HepG2 Cell Detection *Nanoscale* **7 3627–3633**

[6] Zheng Y, Wang W, Fu Q, Wu M, Shayan K, Wong K M, Singh S, Schober A, Schaaf P and Lei Y 2014 Surface-Enhanced Raman Scattering (SERS) Substrate Based on Large-

Area Well-Defined Gold Nanoparticle Arrays with High SERS Uniformity and Stability *Chempluschem.* **79 1622–1630**

[7] Wen L Y, Wang Z J, Mi Y, Xu R, Yu S H and Lei Y 2015 Designing heterogeneous one-dimensional nanostructure arrays by electrochemical deposition for energy conversion and storage *Small* **11 3408–3428**

[8] Zhan Z B and Lei Y 2014 Sub-100-nm nanoparticle arrays with perfect ordering, tunable and uniform dimensions fabricated by combining nanoimprinting with ultrathin alumina membrane technique *ACS Nano* **8 3862–3868**

[9] Wen L Y, Mi Y, Wang C L, Zhao H P, Grote F, Zhang Z B, Zhou M and Lei Y 2014 Cost-effective atomic layer deposition synthesis of Pt nanotube arrays: application for high performance supercapacitor *Small* **10 3162–3168**

[10] Lei Y, Chim W K, Sun H P and Wilde G 2005 Highly ordered CdS nanoparticle arrays on silicon substrates and photoluminescence properties *Appl. Phys. Lett.* **86 103106**

[11] Ali S M U, Kashif M, Ibupoto Z H, Fakhar-e-Alam M, Hashim U and Willander M 2011 Functionalised zinc oxide nanotube arrays as electrochemical sensors for the selective determination of glucose Micro *Nano Lett*. **6 609–613**

[12] Fu J, Mao P and Han J 2008 Artificial molecular sieves and filters: a new paradigm for biomolecule separation *Trends Biotechnol*. **26 311–320**

[13] Nakayama K, Tanabe K and Atwater H A 2008 Plasmonic nanoparticle enhanced light absorption in GaAs solar cells Appl. Phys. Lett. **93 3–5**

[14] Vallet-Regi M, Izquierdo-Barba I and Colilla M 2012 Structure and functionalization of mesoporous bioceramics for bone tissue regeneration and local drug delivery Philos. Trans. R. Soc. A Math. Phys. Eng. Sci. **370 1400–1421**

[15] Tarish S, Al-Haddad A, Xu R, Cao D, Wang Z, Qu S, Nabi G and Lei Y 2016 The shift of the optical absorption band edge of ZnO/ZnS core/shell nanotube arrays beyond quantum effects *J. Mater. Chem. C* **4 1369–1374**

[16] Tarish S, Wang Z, Al-Haddad A , Wang C , Ispas A, Romanus H, Schaaf P, Lei Y 2015 Synchronous Formation of ZnO/ZnS Core/Shell Nanotube Arrays with Removal of Template for Meliorating Photoelectronic Performance *J. Phys. Chem. C* **119 1575–1582**

[17] Armbruster D A and Pry T 2008 Limit of blank, limit of detection and limit of quantitation *Clin. Biochem. Rev.* **29 (Suppl 1) S49–S52**

[18] Marie M, Mandal S and Manasreh O 2015 An Electrochemical Glucose Sensor Based on Zinc Oxide Nanorods *Sensors* **15 18714–1872**

[19] Tsierkezos N G and Ritter U 2012 Electrochemical Responses and Sensitivities of Films Based on Multi-Walled Carbon Nanotubes in Aqueous Solutions *J. Solution Chem.* **41 2047–2057**

[20] Nicholson R S 1965 Theory and Application of Cyclic Voltammetry f m Measurement of Electrode Reaction Kinetics *Anal. Chem*. **37 1351–1355**

[21] Allan J M 1993 A note on the Randles-Sevcik Function from electrochemistry *AApl.Math. Compu.* **57 305-310**

[22] Cai B, Zhou Y, Zhao M, Cai H, Ye Z, Wang L, Huang J 2014 Synthesis of ZnO–CuO porous core–shell spheres and their application for the non-enzymatic glucose sensor *Appl.*

Phys. A Mater. Sci. Process. **118 989–996**

[23] Weber J, Jeedigunta S and Kumar A 2008 Fabrication and Characterization of ZnO Nanowire Arrays with an Investigation into Electrochemical Sensing Capabilities *J. Nanomate.* **15 1–5**

[24] Deng C, Chen J, Chen X, Xiao C, Nie L, Yao S, 2008 Direct electrochemistry of glucose oxidase and biosensing for glucose based on boron-doped carbon nanotubes modified electrode *Biosens. Bioelectron* **23 1272–1277**

[25] Karuppiah C, Palanisamy S, Chen S M, Veeramani V and Periakaruppan P 2014 Direct electrochemistry of glucose oxidase and sensing glucose using a screen-printed carbon electrode modified with graphite nanosheets and zinc oxide nanoparticles *Microchim. Acta* **181 1843–1850**

[26] Sung Y M, Noh K, Kwak W C and Kim T G 2012 Enhanced glucose detection using enzyme-immobilized ZnO/ZnS core/sheath nanowires. Sensors *Actuators B Chem*. **161 453–459**

[27] Laviron E 1979 General expression of the linear potential sweep voltammogram in the case of diffusionless electrochemical systems *J. Electroanal Chem*. **101 19–28**

[28] Palanisamy S, Cheemalapati S and Chen S M 2012 Enzymatic Glucose Biosensor Based on Multiwalled Carbon Nanotubes-Zinc Oxide Composite *Int. J. Electrochem. Sci* **7 8394–8407**

[29] Janegitz B C, Pauliukaite R, Ghica M E, Brett C M A and Fatibello-Filho O 2011 Direct electron transfer of glucose oxidase at glassy carbon electrode modified with

functionalized carbon nanotubes within a di hexadecyl phosphate film *Sensors Actuators, B Chem* **158 411–417**

[30] Luo X, Killard A J and Smyth M R 2006 Reagentless glucose biosensor based on the direct electrochemistry of glucose oxidase on carbon nanotube-modified electrodes *Electroanalysis.* **18 1131–1134**

[31] Cai C and Chen J 2004 Direct electron transfer of glucose oxidase promoted by carbon nanotubes *Anal. Biochem.* **332 75–83**